




## Effects of fuel decomposition and stratification on the forced ignition of a static flammable mixture

Xinyi Chen<sup>a</sup>, Wenrui Peng<sup>b</sup>, Philippe Gillard<sup>c</sup>, Leo Courty<sup>c</sup>, Mamadou Lamine Sankhe<sup>c</sup>,  
Stephane Bernard<sup>c</sup>, Yun Wu<sup>b</sup>, Yuan Wang<sup>a</sup> and Zheng Chen <sup>a\*</sup>,

<sup>a</sup>SKLTCS, CAPT, BIC-ESAT, College of Engineering, Peking University, Beijing, People's Republic of China <sup>b</sup>Science and Technology on Plasma Dynamics Laboratory, Air Force Engineering University, Xi'an, People's Republic of China <sup>c</sup>Universite d'Orleans, INSA-CVL, PRISME EA 4229, Bourges, France

(Received 15 July 2020; accepted 16 June 2021)

In advanced propulsion systems such as scramjet engines, endothermic decomposition of onboard large hydrocarbon fuels can be used effectively for cooling and active thermal protection. During the cooling process, large hydrocarbon fuels absorb heat and decompose into small fragments. Since fuel decomposition changes the chemical and transport properties of the reactants, it is expected to affect the combustion afterwards. In this study, forced ignition in quiescent n-decane/air mixtures with fuel decomposition is investigated via a simplified model and transient numerical simulations considering detailed chemistry and transport. The emphasis is placed on assessing the effects of fuel decomposition on ignition kernel development and minimum ignition energy (MIE) in both homogenous and fuel-stratified mixtures. Fuel decomposition is modelled by a homogeneous ignition process in n-decane/air mixture at constant atmospheric pressure and with an initial temperature of 1300 K. Small fragments appear during the pyrolysis process. The partially-reacted mixture is frozen and cooled to a lower temperature and used as the initial mixture in forced ignition. For homogeneous mixtures, fuel decomposition can greatly promote ignition for fuel-lean decane/air mixtures while it has little effect for the stoichiometric case. Fuel decomposition also affects the duration of unsteady ignition kernel transition. Besides, fuel decomposition and fuel stratification are combined to further promote forced ignition. New flame regimes are observed and an optimum stratification radius is identified. In order to promote the forced ignition, only the fuel within the optimum stratification radius needs to be decomposed. Furthermore, laser and spark ignition experiments are conducted to measure the MIE of n-decane/ethylene/air mixtures with different equivalence ratios and ethylene blending ratios. The MIE measured in experiments cannot be directly compared with simulation results since the simulation model for forced-ignition is simplified. Nevertheless, the experimental results are consistent with simulation results and thus validate some conclusions mentioned above. The present results provide useful guidance to the fundamental understanding of forced ignition in a mixture with fuel decomposition.

**Keywords:** fuel decomposition; fuel stratification; ignition; minimum ignition energy

### 1. Introduction

In scramjet, thermal management of the overall vehicle is a significant challenge [1,2] since the total temperature of incoming flow can be very high at high flight Mach number

---

\*Corresponding author. Email: [cz@pku.edu.cn](mailto:cz@pku.edu.cn)

This article has been corrected with minor changes. These changes do not impact the academic content of the article.

[3]. In practical engines, it is common to cool the combustor with the onboard fuel in order to reduce the weight of cooling system and to increase the thermal efficiency through heat recovery [1]. During the cooling process, hydrocarbon fuels absorb heat and undergo pyrolysis through endothermic reactions. Consequently, the heavy hydrocarbons could decompose into light gaseous species including hydrogen, methane, ethylene, and butane [4]. Besides, it was found that for flames propagating in large-hydrocarbon/air mixtures, fuel pyrolysis occurs in the preheat zone within a temperature range of 1050–1450 K [5] and that the typical time scale for the overall decomposition process is within 1 ms [4,6]. Therefore, it is necessary to understand how fuel decomposition/pyrolysis affects the fundamental combustion processes such as ignition, flame propagation and stabilisation.

Though extensive studies have been conducted to characterise the fuel decomposition process [4–8], there are only a few studies on how fuel decomposition affects ignition and flame propagation. Smolke et al. [5] assessed the effects of n-dodecane decomposition on its mass burning rate and extinction strain rate. They found that the mass-burning rate is only slightly increased by fuel decomposition while the density-weighted extinction strain rate is notably more sensitive to fuel decomposition under fuel-lean and stoichiometric conditions. Zhong and Peng [9] found that the cracking of large hydrocarbon fuels cannot greatly increase the laminar flame speed and thereby has little effect on the combustion in a practical combustor.

To the authors' knowledge, the effects of fuel decomposition on the transient forced ignition process have not been studied before. Forced ignition is one of the most fundamental combustion processes [10]. Unlike autoignition, forced ignition strongly depends on the mass diffusivity of the reactant [11–13]. Since the decomposed small fragments have much larger mass diffusivity compared to the original hydrocarbon fuel, fuel decomposition is expected to strongly affect the forced ignition process. This motivates the present work, which aims to assess the effects of fuel decomposition on the ignition kernel propagation and minimum ignition energy (MIE).

Besides, in practical combustion facilities, perfectly homogenous mixture is difficult to be achieved and non-uniform spatial distribution of mixtures always exists. Previous studies have shown that fuel-stratification has the advantages in improving flame stability [14] and extending lean flammability [15]. Recently, Wang et al. [16] has demonstrated that fuel stratification can greatly promote the forced ignition in fuel-lean n-decane/air mixtures. This is because the ignition kernel develops much more easily in a mixture with lower Lewis number. As mentioned before, fuel decomposition helps to increase the mass diffusivity and thereby reduce the effective Lewis number. Therefore, the combination of fuel decomposition and fuel stratification is expected to promote forced ignition. This is also investigated in the present work.

The objective of this study is to assess the effects of fuel decomposition on forced ignition in homogenous and fuel-stratified mixtures. N-decane/air mixtures are considered in this study since n-decane is popularly used as a component in surrogate jet fuels. Transient numerical simulations considering detailed high-temperature chemistry as well as temperature-dependent thermal and transport properties are conducted. Moreover, the laser and spark ignition experiments are conducted to validate the conclusions drawn from simulation results.

It is noted that the forced ignition process in practical combustion engines is extremely complex since it consists of complicated plasma formation, spark-induced shock wave, turbulence-chemistry interaction, etc. As a crucial first step to assess the effects of fuel decomposition and stratification, here we consider forced ignition caused by heat

deposition in a static flammable mixture. Including additional physics such as flow and turbulence and their effects on ignition are outside of the scope of this study and need to be explored in future studies.

## 2. Numerical model and methods

Here, we consider the simulations of forced ignition process induced by energy deposition in n-decane/air mixtures. The one-dimensional computational domain is  $0 \leq r \leq 25$  cm in a spherical coordinate. It is initially filled with static mixture at a temperature of  $T_0 = 400$  K and pressure of  $P_0 = 1$  atm. At both boundaries,  $r = 0$  and 25 cm, zero flow velocities and zero gradients of mass fractions and temperature are enforced.

The transient forced ignition process is simulated using the in-house code A-SURF [12,17,18]. A-SURF solves the following conservation equations (including species, momentum and energy conservation equations) for one-dimensional, adiabatic, multi-component, reactive flow in a spherical coordinate:

$$\frac{\partial U}{\partial t} + \frac{\partial F(U)}{\partial r} + 2 \frac{G(U)}{r} = F_v(U) + S_R \quad (1)$$

where  $t$  and  $r$  are the temporal and spatial coordinates respectively. The vectors  $U$ ,  $F(U)$ ,  $G(U)$ ,  $F_v(U)$ , and  $S_R$  are defined as:

$$\begin{aligned} U &= \begin{pmatrix} \rho Y_1 \\ \rho Y_2 \\ \vdots \\ \rho Y_n \\ \rho u \\ E \end{pmatrix}, F(U) = \begin{pmatrix} \rho u Y_1 \\ \rho u Y_2 \\ \vdots \\ \rho u Y_n \\ \rho u^2 + P \\ (E + P)u \end{pmatrix}, G(U) = \begin{pmatrix} \rho u Y_1 \\ \rho u Y_2 \\ \vdots \\ \rho u Y_n \\ \rho u^2 \\ (E + P)u \end{pmatrix}, \\ F_v(U) &= \begin{pmatrix} -r^{-2}(r^2 \rho Y_1 V'_1)_r \\ -r^{-2}(r^2 \rho Y_2 V'_2)_r \\ \vdots \\ -r^{-2}(r^2 \rho Y_n V'_n)_r \\ r^{-2}(r^2 \tau_1)_r - \frac{2\tau_2}{r} \\ r^{-2}q_r + \Phi \end{pmatrix}, S_R = \begin{pmatrix} \omega_1 \\ \omega_2 \\ \vdots \\ \omega_n \\ 0 \\ 0 \end{pmatrix} \end{aligned} \quad (2)$$

in which  $\rho$  is the density,  $Y_k$  the mass fraction of the  $k$ th species,  $u$  the radial flow velocity and  $E$  the total energy per unit mass. Instead of solving the continuity equation, the species conservation equations for all  $n$  species are solved in A-SURF. The continuity equation is recovered from the summation of all species conservation equations. In the species conservation equations, the subscript  $r$  in  $F_v(U)$  represents the partial derivative with respect to  $r$ .  $\omega_k$  and  $V'_k$  are the production rate and diffusion velocity of species  $k$ , respectively. The production rate  $\omega_k$  is specified via collection of elementary reactions and the species diffusion velocity  $V'_k$  is evaluated based on the mixture-averaged model. A correction term for the diffusion velocity of each species is included so that the summation of all species conservation equations yields the continuity equation. CHEMKIN [19] and TRANSPORT [20] packages are incorporated into A-SURF to calculate the thermodynamic and transport properties. In simulations, the pyrolysis and oxidation of n-decane are modelled using the

high-temperature mechanism of Chaos et al. [21], which contains of 54 species and 382 elementary reactions.

In the momentum equation,  $P$  is the pressure and the viscous stresses,  $\tau_1$  and  $\tau_2$ , are defined as:

$$\tau_1 = 2\mu \frac{\partial u}{\partial r} - \frac{2}{3}\mu \frac{1}{r^2} \frac{\partial(r^2 u)}{\partial r}, \quad \tau_2 = 2\mu \frac{u}{r} - \frac{2}{3}\mu \frac{1}{r^2} \frac{\partial(r^2 u)}{\partial r} \quad (3)$$

where  $\mu$  is the dynamic viscosity of the mixture.

In the energy conservation equation, the total energy,  $E$ , is defined via:

$$E = -P + \frac{\rho u^2}{2} + \rho h, h = \sum_{k=1}^n (Y_k h_k), h_k = h_{k,0} + \int_{T_0}^T C_{P,k}(T) dT \quad (4)$$

where  $h_k$  is the enthalpy of the  $k$ th species,  $h_{k,0}$  the species formation enthalpy at the reference temperature  $T_0$ , and  $C_{P,k}$  the specific heat of the  $k$ th species at constant pressure. The heat flux  $q$  is:

$$q = r^2 \left[ \lambda \frac{\partial T}{\partial r} - \rho \sum_{k=1}^n (h_k Y_k V'_k) \right] \quad (5)$$

in which  $\lambda$  is the thermal conductivity of the mixture.  $\Phi$  is the viscous dissipation rate, which is defined through:

$$\Phi = \mu \left\{ 2 \left( \frac{\partial u}{\partial r} \right)^2 + 4 \left( \frac{u}{r} \right)^2 - \frac{2}{3} \left[ \frac{1}{r^2} \frac{\partial(r^2 u)}{\partial r} \right]^2 \right\} + u \left[ \frac{1}{r^2} \frac{\partial(r^2 \tau_1)}{\partial r} - 2 \frac{\tau_2}{r} \right] \quad (6)$$

The pressure can be obtained from the density, temperature and mean molecular weight using the ideal gas state equation:

$$P = \frac{\rho R T}{\bar{M}} \quad (7)$$

where  $R = 8.314 \text{ J/(mol}\cdot\text{K)}$  is the universal gas constant.

The finite volume method is used to discretize the governing equations (1). The second-order accurate, Strang splitting fractional-step procedure is utilised to separate the time evolution of the stiff reaction term  $S_R$  from that of the convection and diffusion terms. In the first fractional step, the non-reactive flow is solved by employing Runge–Kutta, MUSCL-Hancock, and central difference schemes, all of second-order accuracy, for the calculation of temporal integration, convective flux, and diffusive flux, respectively. The chemistry is solved in the second fractional step for a homogeneous system at each grid using the VODE solver [22]. Dynamically adaptive mesh refinement is employed and the reaction front is always fully covered by the finest mesh with a size of  $7.8 \mu\text{m}$ . Numerical convergence is checked and ensured by further decreasing the time step and mesh size in simulation. ASURF has been successfully used in previous studies on ignition and flame propagation [16,23–25].

In simulations, the mixture is centrally ignited through energy deposition given by the following source term in the energy equation [26]:

$$q_{ig}(r, t) = \begin{cases} \frac{E_{ig}}{\pi^{1.5} r_{ig}^3 \tau_{ig}} \exp\left[-\left(\frac{r}{r_{ig}}\right)^2\right] & \text{if } t < \tau_{ig} \\ 0 & \text{if } t \geq \tau_{ig} \end{cases} \quad (8)$$

where  $E_{ig}$  is the total input ignition energy,  $\tau_{ig}$  the duration of energy deposition, and  $r_{ig}$  the radius of the energy deposited region. In simulations, the MIE is obtained by the method of

trial and error with error below 2%. Previous studies [10,27] showed that the MIE depends on both  $\tau_{ig}$  and  $r_{ig}$ . Similar to our previous work [16], the duration and radius of ignition energy deposition are fixed to be  $\tau_{ig} = 0.5$  ms and  $r_{ig} = 0.5$  mm, respectively.

Fuel decomposition is studied in a homogeneous adiabatic and isobaric process following the same methodology proposed by Smolke et al. [5]. The pyrolysis of homogeneous  $nC_{10}H_{22}$ /air mixtures is modelled under isobaric and adiabatic conditions at the same atmospheric pressure but a high initial temperature of  $T_{P,0} = 1300$  K. During the transient homogeneous pyrolysis process, the species concentrations evolve and they are frozen at a certain value of fuel decomposition fraction,  $C$ , which is defined as the percentage of fuel decomposed. The frozen mixture is then cooled to a temperature  $T_i$  to match the enthalpy of the initial undecomposed  $nC_{10}H_{22}$ /air mixture at  $T_0 = 400$  K [5]. Then this frozen mixture at  $T_i$  is used as the initial reactant in the transient ignition simulation.

Moreover, we also consider forced ignition in a fuel-stratified mixture: the ignition kernel first develops in a fuel-decomposed mixture and then it propagates into an  $n$ -decane/air mixture without fuel decomposition. The initial molar fraction distribution for the  $i$ th specie is specified by the following hyperbolic tangent function [16]:

$$x^i(r, t = 0) = \frac{x_{in}^i + x_{out}^i}{2} - \frac{x_{in}^i - x_{out}^i}{2} \tanh\left(\frac{r - R_S}{\delta}\right) \quad (9)$$

where  $x_{in}$  and  $x_{out}$  are respectively the inner and outer molar fractions of the  $i$ th species,  $R_S$  the stratification radius, and  $\delta$  the mixing layer thickness. Same as the case of homogeneous mixture, the mixture composition (i.e. the values of  $x_{in}^i$ ) in the inner zone is determined by fuel decomposition fraction  $C$  and its temperature  $T_i$  is calculated based on the constant total enthalpy [5]. The mixture composition in the outer zone,  $x_{out}^i$ , is determined by the equivalence ratio and there is no fuel decomposition. In the inner and outer zones, the mixtures have the same equivalence ratio. In all simulations, the mixing layer thickness is fixed to be  $\delta = 0.04$  mm. Consequently, fuel stratification is characterised only by three parameters: the stratification radius  $R_S$ , the equivalence ratio  $\phi$  and the fuel decomposition fraction  $C$  in the inner zone.

### 3. Numerical results and discussion

#### 3.1. Pyrolysis of $n$ -decane in an isobaric homogeneous system

We first model the pyrolysis and oxidation of  $n$ -decane/air under homogeneous isobaric and adiabatic conditions. The results are shown in Figures 1 and 2.

According to previous studies [5,28], first  $n$ -decane decomposes through the break of C–C bond. Then  $C_2H_4$  is produced through  $\beta$ -scission via alkyl radicals and H-abstraction by OH radicals. As shown in Figure 1, the typical time for complete decomposition of  $n$ -decane is around 0.3 ms at the cracking temperature of  $T_{P,0} = 1300$  K. In the early stage, the temperature decreases slightly due to the endothermic decomposition of large hydrocarbon molecules. With the growth of radical pool, the system is dominated by exothermic oxidation which leads to temperature rise. During the pyrolysis process, the concentration of  $C_2H_4$  increases continuously.

In consistent with previous work [6], Figure 2 shows that the mainly products from  $nC_{10}H_{22}$  decomposition are mainly  $CH_4$ ,  $H_2$ , and small alkene ( $C_nH_{2n}$  with  $n = 2, 3$  and 4) fragments. Their mass fractions are normalised by the initial mass fraction of  $nC_{10}H_{22}$ .

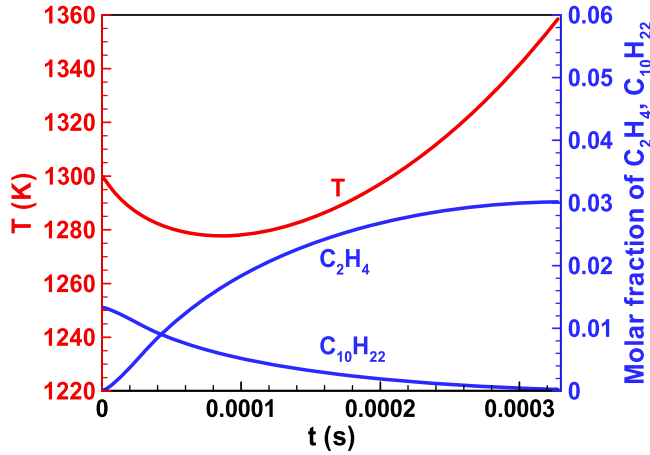


Figure 1. Evolution of temperature and molar fractions of  $C_2H_4$  and  $nC_{10}H_{22}$  during homogeneous ignition of stoichiometric  $nC_{10}H_{22}/air$  at  $T_{p,0} = 1300$  K and  $P = 1$  atm.

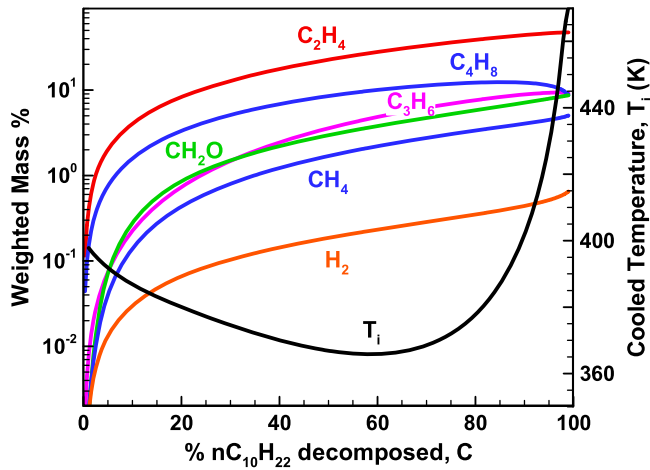


Figure 2. Mass percentages of key products and cooled temperature computed for  $nC_{10}H_{22}$  decomposition in air with  $\phi = 1.0$ ,  $T_{p,0} = 1300$  K and  $P = 1$  atm.

Being the most abundant intermediate, the weighted mass of  $C_2H_4$  is about one magnitude larger than other products. On one hand, fuel decomposition produces lighter and more reactive fragments. On the other hand, the temperature decreases due to endothermic decomposition reactions. These two factors are coupled and compete with each other. Their overall effects on forced ignition are assessed in the following two sub-sections.

It is worth noting that in practical scramjet, large hydrocarbons undergo thermal cracking reactions first before they are injected into the combustor and mixed with the supersonic incoming flow [2]. Therefore, fuel pyrolysis in real engines is not exactly a homogeneous ignition process of premixed mixture. In our study, an ideal partial oxidation model is used here in order to get a simplified fundamental scientific problem. As observed by You et al. [6] and Malewicki et al. [29,30], during the homogenous ignition process, obvious oxygen decay begins after most of the fuel decomposes. This suggests that pyrolytic reactions of

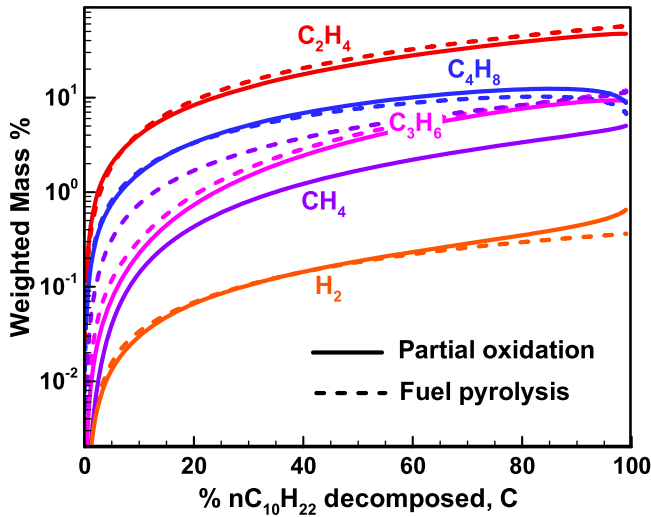


Figure 3. Comparison of mass percentages of key products computed for  $nC_{10}H_{22}$  decomposition in air with  $\phi = 1.0$  and  $nC_{10}H_{22}$  pyrolysis at  $T = 1300$  K and  $P = 1$  atm.

the fuel are mostly responsible for fuel decay during the partial oxidation process. A quantitative comparison of mass fractions of pyrolysis products from partial oxidation and fuel pyrolysis is made in Figure 3. The n-decane pyrolysis is modelled under homogenous isobaric and isothermal conditions at a fixed temperature of  $T = 1300$  K, which is consistent with thermal cracking experiments in previous studies [6,31]. It is shown that the main products are in comparable amount in these two models, except for the subordinate species such as  $CH_4$ . That is because during the partial oxidation process, some of  $CH_4$  are converted to  $CH_2O$  and other radicals by oxidation reactions. As will be discussed later, the concentrations of subordinate pyrolysis products have a minor effect on the ignition process. Therefore, it is reasonable to study the fuel pyrolysis through homogenous ignition process.

Besides, unlike the autoignition process which is fully controlled by chain-initiation and chain-branching reactions and thereby is greatly affected by the appearance of radical, the forced-ignition process considered in the present work is mainly heat balance around the ignition kernel and thereby the appearance of small amount of radical is expected to have weaker influence on the MIE than on the autoignition delay time.

### 3.2. Forced ignition in a homogenous mixture

In this subsection, we assess the effects of fuel decomposition on forced ignition in an initially homogenous mixture (i.e. initially the mixture composition is the same at every position).

Figure 4(a) shows the propagation speeds of ignition kernels/spherical flames initiated by different ignition energies in a fuel-lean ( $\phi = 0.7$ )  $nC_{10}H_{22}$ /air mixture without fuel decomposition (i.e.  $C = 0$ ). In simulation, the flame radius,  $R_f$ , is defined as the location where local maximum heat release rate occurs, and the flame propagation speed is obtained from numerical differentiation according to  $S_b = dR_f/dt$ . Figure 4(b) shows the change of flame propagation speed with the stretch rate, which is  $K = 2S_b/R_f$  for propagating

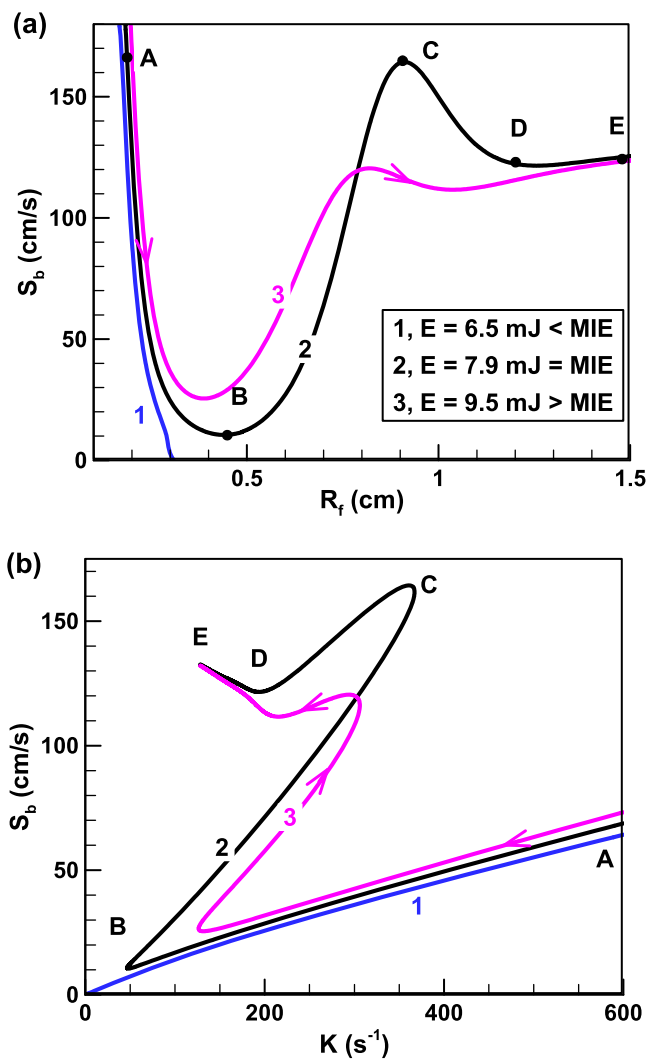


Figure 4. Change of the flame propagation speed with flame radius and stretch rate for an  $nC_{10}H_{22}$ /air mixture with  $\phi = 0.7$  and different ignition energies.

spherical flames. The MIE is  $E_{min} = 7.9 \text{ mJ}$  and successful ignition can only be achieved for  $E \geq E_{min}$ . Similar to previous studies [16,32,33], four distinct flame regimes are observed for the successful ignition case: spark-assisted ignition kernel propagation regime (AB in Figure 4), unsteady flame transition regime (BC), overdriven flame propagation regime (CD), and quasi-steady flame propagation regime (DE).

The effects of fuel decomposition on ignition kernel and spherical flame propagation are shown in Figure 5. Different  $S_b$ - $K$  curves are obtained for fuel-lean  $nC_{10}H_{22}$ /air mixtures with different fuel decomposition fractions. The ignition energy is chosen to be the MIE for each case:  $E = E_{min} = 7.9 \text{ mJ}$  for  $C = 0\%$ ,  $E = E_{min} = 2.3 \text{ mJ}$  for  $C = 30\%$ , and  $E = E_{min} = 1.06 \text{ mJ}$  for  $C = 50\%$ , indicating that the MIE decreases dramatically as the fuel decomposition fraction increases.



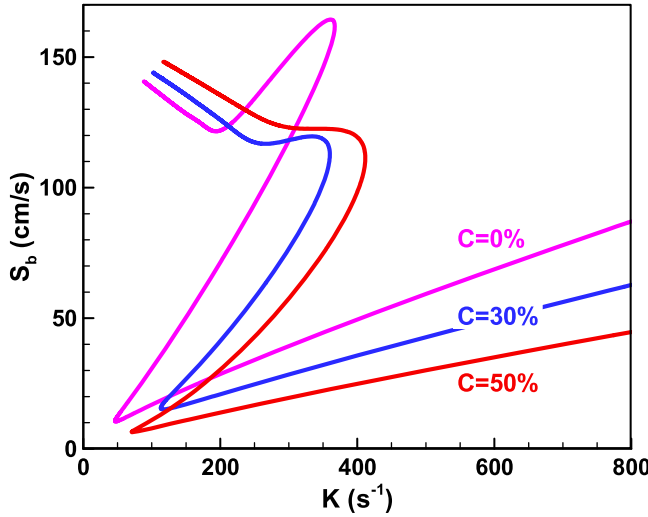


Figure 5. Flame propagation speed  $S_b$  as a function of stretch rate  $K$  for fuel-lean  $nC_{10}H_{22}/air$  ( $\phi = 0.7$ ) with different fuel decomposition fractions.

In spark-assisted ignition kernel propagation regime, the flame propagation strongly depends on the ignition energy. Since the ignition energy decreases from  $E = 7.9$  mJ for  $C = 0\%$  to  $E = 1.06$  mJ for  $C = 50\%$ , the ignition kernel propagates much slower at higher fuel decomposition fraction. The propagation speed of the ignition kernel decays quickly since the excess enthalpy from the ignition energy becomes lower at larger flame radius [32]. Then the ignition kernel evolves into the unsteady flame transition regime, in which flame propagation is mainly driven by chemical reactions and transport. With the increase of fuel decomposition, the effective Lewis number of the mixture becomes smaller, corresponding to a normal flame with smaller flame thickness and higher flame speed. Figure 5 shows that with the increase of fuel decomposition, the duration of unsteady flame transition becomes shorter. This is because of the increase in the radical concentration after fuel cracking, which accelerates the transition process. Moreover, in Figure 5 the overdriven flame regime is clearly shown for  $C = 0\%$ , while it becomes less obvious for  $C = 50\%$ . This is due to the shorter duration of the reaction acceleration and the smaller Lewis number of the fragments from fuel decomposition. When the over-driven flame accelerated to the peak flame propagation speed, it slows down and transits into a quasi-steady flame propagating outwards.

In order to quantify the fuel decomposition effects on forced ignition, the MIEs are calculated for different values of equivalence ratio and fuel decomposition fraction. The results are summarised in Figure 6. Besides  $C_{10}H_{22}/air$  with fuel decomposition, Figure 6(a) also shows the results for  $C_{10}H_{22}/C_2H_4/air$  without fuel decomposition, which will be discussed in Section 4. Figure 6(a) shows that for a stoichiometric  $nC_{10}H_{22}/air$  mixture, the MIE remains nearly constant, indicating that fuel decomposition has little effect on its MIE. However, substantial reduction in the MIE is observed for the fuel-lean case with  $\phi = 0.7$ : for 70% n-decane decomposition (i.e.  $C = 70\%$ ), the MIE decreases to be about one-tenth of that for the case without fuel decomposition (i.e.  $C = 0\%$ ). Therefore, fuel decomposition can greatly promote ignition for fuel-lean  $nC_{10}H_{22}/air$  mixtures. Besides, it is noticed that there exists a lower limit of MIE around 0.75 mJ.

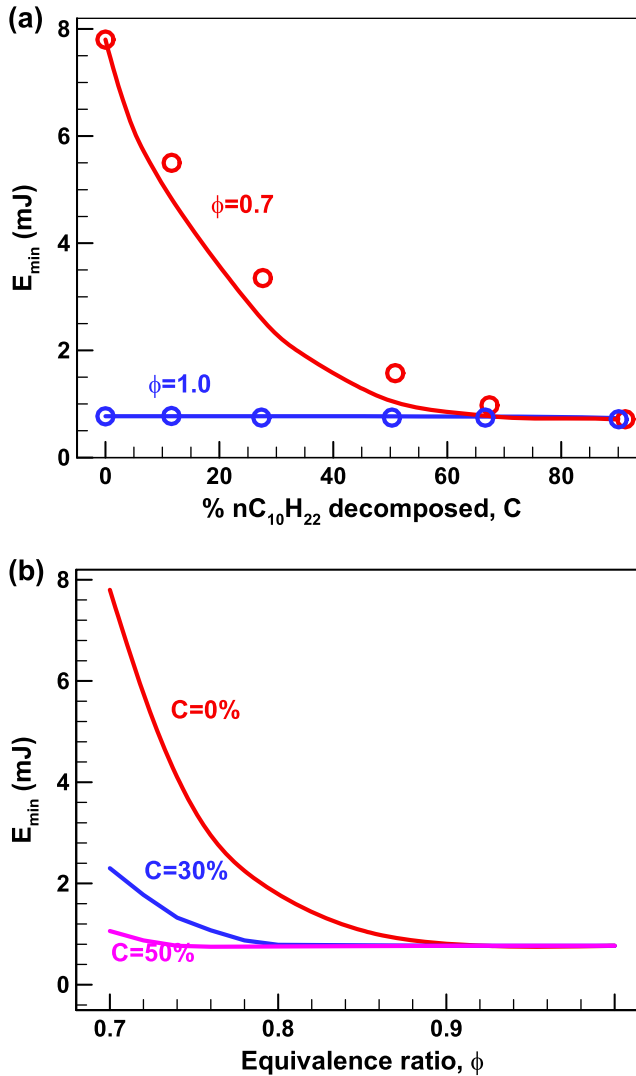


Figure 6. Change of the MIE with (a) fuel decomposition fraction and (b) equivalence ratio. The lines are results for  $C_{10}H_{22}/air$  with fuel decomposition. The symbols represent results for  $[(1-\alpha)C_{10}H_{22} + \alpha C_2H_4]/air$  without fuel decomposition; and the symbols from the left to the right are respectively for  $\alpha = 0, 0.2, 0.4, 0.6, 0.7$  and  $0.8$ .

Once the MIE decreases to this limit, further fuel decomposition does not help to reduce the MIE.

Figure 6(b) shows that for the case without fuel decomposition (i.e.  $C = 0\%$ ), the MIE first decreases dramatically with the increase of the equivalence ratio and then it approaches a constant value. Similar trend was observed in previous studies [10,12,27]. With the increase of fuel decomposition, the dependence of the MIE on equivalence ratio becomes weaker. This is because more fuel decomposition results in lower effective Lewis number (or Markstein length) and weaker stretch effect on the propagation of the ignition kernel which has high stretch rate [17].

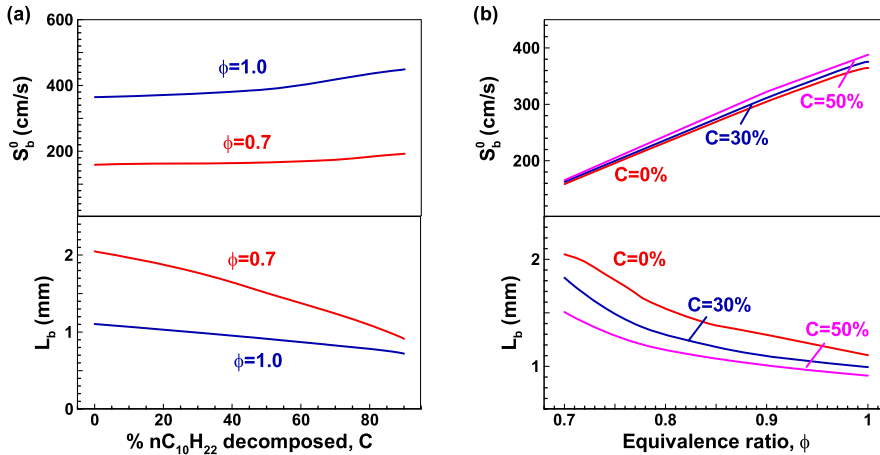


Figure 7. Change of the unstretched flame propagation speed and Markstein length with (a) fuel decomposition fraction and (b) equivalence ratio.

In Figure 7, the Markstein length,  $L_b$ , and the unstretched flame propagation speed,  $S_b^0$ , are obtained from the linear relationship between  $S_b$  and  $K$  in the quasi-steady flame propagation regime [34,35]. As expected, the unstretched flame propagation speed increases monotonically with the increase of fuel decomposition and the equivalence ratio, while the Markstein length shows an opposite trend. This implies that the ignition kernel is less sensitive to the stretch at the initial stage and can obtain a higher initial speed to propagate outwardly, which makes ignition occur more easily. Besides, the Markstein length of the mixture is shown to be reduced by fuel decomposition. Therefore, the thermal-diffusion instability becomes stronger and the cellular structure appears earlier for higher fuel decomposition.

Figure 8 plots the MIE as a function of Markstein length for different values of equivalence ratio ( $\phi = 0.7-1.0$ ) and fuel decomposition ( $C = 0\%-90\%$ ). The MIE is shown to decrease exponentially with the decrease of the Markstein length. The results at different equivalence ratios and fuel decomposition fractions are shown to almost collapse onto a single curve. Therefore, the MIE can be quantified by the Markstein length.

Figures 6 and 8 show that the increase in both fuel decomposition and equivalence ratio can reduce the MIE. Therefore, the combination of fuel decomposition and fuel stratification is expected to further promote forced ignition, which is investigated in the following subsection.

### 3.3. Forced ignition in a fuel-stratified mixture

As mentioned previously, fuel stratification is characterised by the following three parameters: the stratification radius  $R_s$ , the equivalence ratio  $\phi$  and the fuel decomposition fraction  $C$  in the inner zone. Since the effects of equivalence ratio have been extensively investigated in previous studies [16,36,37], here the equivalence ratio is fixed to be  $\phi = 0.7$  and the emphasis is placed on assessing and interpreting the influence of the other two parameters.

A typical flame propagation process for fuel-stratified  $nC_{10}H_{22}$ /air mixture with fuel decomposition is shown in Figure 9. In addition to the four distinct flame regimes discussed

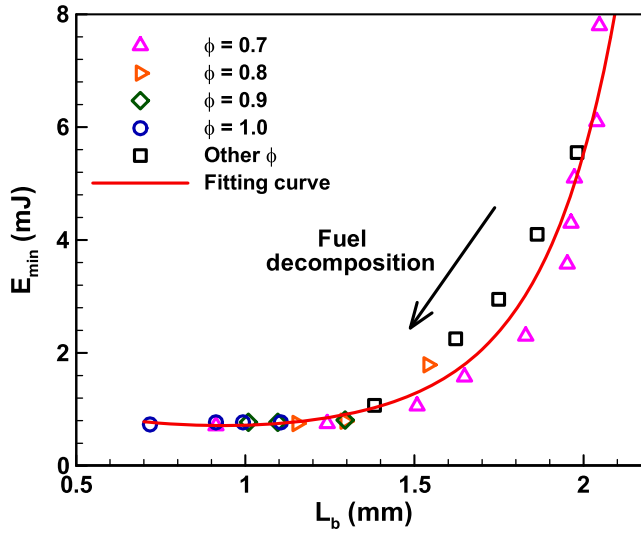


Figure 8. Change of the MIE with burned Markstein length for  $C_{10}H_{22}/air$  with fuel decomposition.

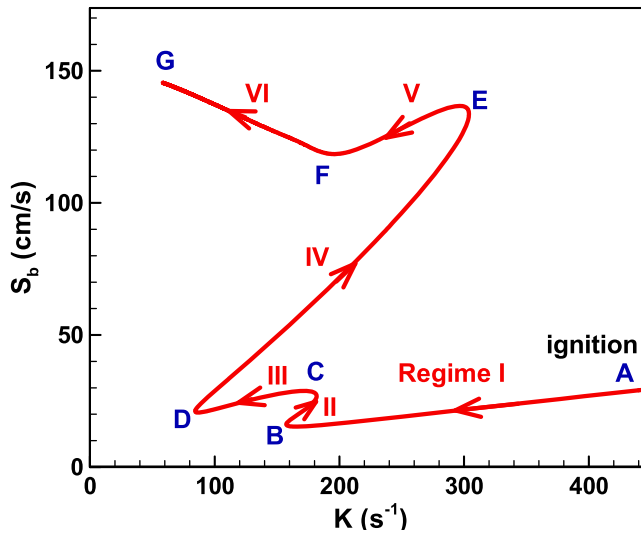


Figure 9. Change of the flame propagation speed with stretch rate for fuel-stratified  $nC_{10}H_{22}/air$  with  $\phi = 0.7$ ,  $C = 50\%$ ,  $E = 1.2$  mJ and  $R_s = 4.0$  mm.

in the previous section, two new flame regimes are induced by fuel stratification. In Figure 9, Regimes I, IV, V and VI respectively correspond to the spark-assisted ignition kernel propagation regime, the unsteady flame transition regime, the overdriven flame regime, and the quasi-steady flame propagation regime. Flame propagations in Regimes II and IV are driven by chemical reactions without the assistance of the ignition energy. Regime II is referred as the first unsteady ignition regime. However, as the flame approaches to the stratification radius, chemical reactions in Regime II slow down due to fuel stratification. Therefore, a subsequent decrease in flame propagation speed is observed

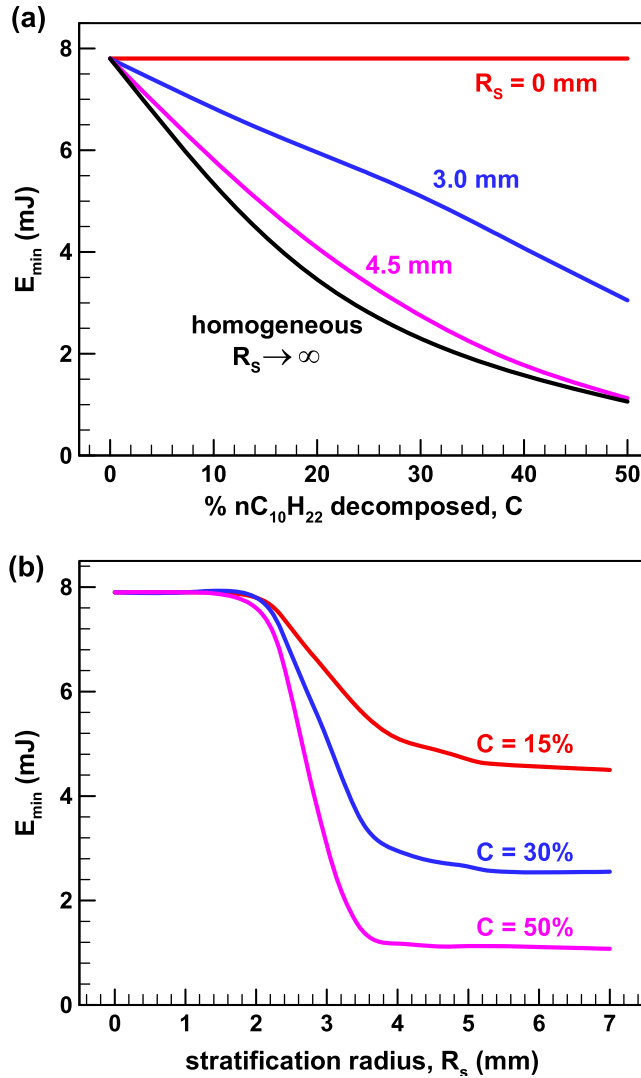


Figure 10. Change of the MIE with (a) fuel decomposition fraction and (b) stratification radius for fuel-stratified  $nC_{10}H_{22}$ /air with  $\phi = 0.7$ .

in regime III, which is called as the fuel-stratification-induced ignition kernel propagation regime. Then the flame propagates into Regime IV. After passing the overdriven flame regime V, it propagates outwardly in a quasi-steady manner in regime VI.

The above results show that fuel decomposition and stratification can greatly change the ignition kernel propagation and flame regimes. Then it is expected that fuel decomposition and stratification can also affect the MIE. The MIEs for the different values of stratification radius and fuel decomposition fraction are calculated and plotted in Figure 10.

Figure 10 depicts the change of the MIE with fuel decomposition fraction in the inner zone and stratification radius. The largest fuel decomposition fraction considered here is  $C = 50\%$ . Similar to the homogenous case, reduction in the MIE is observed due

to fuel stratification. For a fixed stratification radius, the MIE decreases with the fuel decomposition. The case of  $R_S = 0$  mm corresponds to the homogenous mixture without fuel decomposition, and thereby the MIE is constant,  $E_{min} = 7.9$  mJ, as shown by the red line in Figure 10(a). The case of  $R_S = \infty$  corresponds to the homogenous mixture with fuel decomposition. Therefore, the results for  $R_S = \infty$  are the same as those in Figure 6(a) for homogenous mixtures with  $\phi = 0.7$ . Figure 10 shows that for a stratification radius of  $R_S = 3.0$  mm, the MIE decreases linearly with fuel decomposition. When the stratification radius is increased to  $R_S = 4.5$  mm, the results are close to those for homogenous mixtures with  $R_S = \infty$ . Therefore, in order to promote the forced ignition, only the fuel around the ignition kernel needs to be decomposed.

The influence of stratification radius is further examined in Figure 10(b). It is observed that for a given fuel decomposition fraction, there exists a threshold value for the stratification radius. Reduction in the MIE can be achieved only for stratification radius larger than this threshold value. With the increase of stratification radius, the MIE decreases dramatically and eventually approaches to a nearly constant value. The smallest MIE appears to be 4.5 mJ for  $C = 15\%$  at  $R_S = 7$  mm, 2.55 mJ for  $C = 30\%$  at  $R_S = 5.5$  mm and 1.075 mJ at  $R_S = 4.5$  mm for  $C = 50\%$ , which corresponds to the MIE in homogenous mixtures with fuel decomposition. Therefore, for a fixed extent of fuel decomposition, there is an optimum stratification radius. Once the stratification radius increases to this optimum value, further increase does not help to enhance the ignition. The above results indicate that the optimum stratification radius increases when the fuel decomposition fraction decreases.

The above results demonstrate that the combination of fuel decomposition and fuel stratification can promote forced ignition. Substantial reduction in the MIE can be achieved by increasing the fuel decomposition in the inner zone. Moreover, choosing a proper value of stratification radius is of particular importance for the ignition enhancement.

#### 4. Experimental validation

To validate the conclusions drawn from simulation results, experiments are conducted to measure the MIE. However, it is difficult to quantitatively control the fuel decomposition in our experiments. Instead of  $C_{10}H_{22}$ /air with fuel decomposition, in experiments we consider  $[(1-\alpha)C_{10}H_{22} + \alpha C_2H_4]$ /air without fuel decomposition where  $\alpha$  represents the molar fraction of ethylene in the n-decane/ethylene blends. As shown in Figures 1 and 2, large amount of ethylene is produced and ethylene is the main product from n-decane pyrolysis. Therefore, addition of ethylene into n-decane is used to mimic n-decane decomposition. The validation is divided into two steps: first, Figure 6(a) compares the MIEs of two mixtures:  $C_{10}H_{22}$ /air with fuel decomposition, and  $[(1-\alpha)C_{10}H_{22} + \alpha C_2H_4]$ /air without fuel decomposition in numerical simulations. By this treatment, the effects of radicals and other subordinate products from n-decane pyrolysis are eliminated. For each fuel decomposition fraction,  $C$ , there is a corresponding blending ratio  $\alpha$  so that the mass fraction of ethylene in these two mixtures is the same. Figure 6(a) shows that there is a very good agreement between the MIEs for these two mixtures. This indicates that the concentrations of subordinate pyrolysis products have a minor effect on the ignition process. Therefore, it is reasonable to study the fuel-decomposition-induced ignition enhancement through changing the ethylene blending ratio in  $C_{10}H_{22}/C_2H_4$ /air mixtures without fuel decomposition.

Then two types experiments, laser ignition [38–40] and spark ignition [41], are conducted to measure the MIE of  $[(1-\alpha)C_{10}H_{22} + \alpha C_2H_4]$ /air without fuel decomposition.

Reactive mixture is made of vaporised n-decane mixed with ethylene and synthetic air (21%  $O_2$  and 79%  $N_2$ ). The energies giving an ignition probability of 50% ( $E_{50}$ ) of  $C_{10}H_{22}/C_2H_4$ /air mixtures are measured at different equivalence ratios and different ethylene proportions to validate the model.

The laser ignition experiments are performed on the LIQUIM (Laser Ignition of QUIEscent Mixture) setup of the PRISME Laboratory. Vaporised n-decane from Alfa-Aesar (99% pure) is mixed in the reactor with ethylene and synthetic air. Three equivalence ratios are investigated: 0.7, 1 and 1.2 and  $\alpha$  is varied between 0 and 0.7. Initial temperature and absolute pressure are set respectively at 350 K and 1 atm for all experimental conditions. Ignition is obtained by a Quantel Brilliant Nd:YAG laser operating at 1064 nm with variable energies, from hundreds of  $\mu J$  to 150 mJ. Energies are measured by two joulemeters (Ophir Nova) which enables the evaluation of absorbed energy fraction inside the vessel. More details and schemes of the setup are available in [38–40]. In this configuration, waist (beam diameter at the focal spot) is of 19.76  $\mu m$ . Pressure sensor (Kistler 603 B) signals allow to determine whether successful ignition is achieved.  $E_{50}$  is determined using the Langlie method fitted with a log-normal statistical law. With this method,  $E_{50}$  is obtained with around 20 shots. Results are given considering incident energies.

The spark ignition experiments are conducted at Air Force Engineering University in Xi'an. The details on the setup are shown in [41]. The  $C_{10}H_{22}/C_2H_4$ /air mixture is at 400 K and 1 atm. The ignition device consists of a DC power supply with a maximum voltage of 20 kV and capacitors whose capacitances are in the range from 200 nf to 0.1  $\mu f$ . The ignition energy is in the range of 5–500 mJ.  $E_{50}$  is determined by a regression curve derived from the ignition probability model established by the logistic regression model [41].

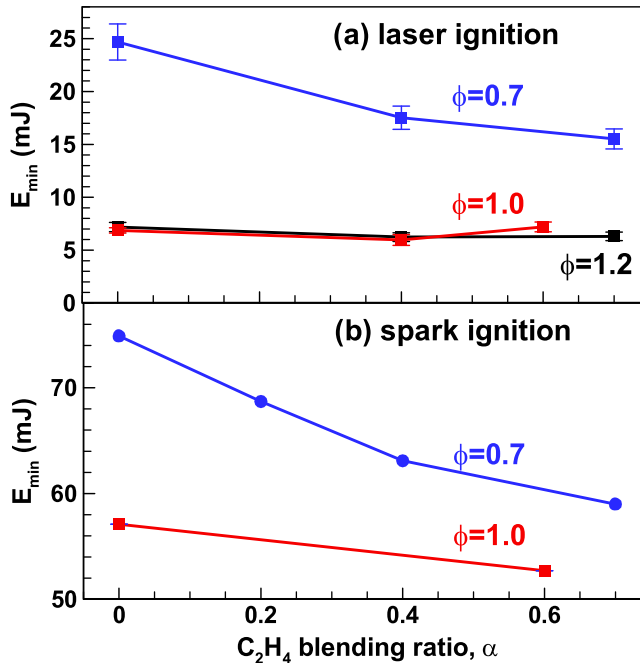


Figure 11. The MIE measured for  $[(1-\alpha)C_{10}H_{22} + \alpha C_2H_4]$ /air mixtures without fuel decomposition: (a) laser ignition; (b) spark ignition.

The experimental results are shown in Figure 11. The MIE measure from spark ignition is much higher than that from laser ignition since large amount of ignition energy goes to the electrodes in spark ignition experiments. Figure 11 shows that ethylene blending has little effect on the MIE for  $\phi = 1.0$  while it can obviously reduce the MIE for  $\phi = 0.7$ . These trends are the same as those from simulations as shown in Figure 6(a). Therefore, the experiments further demonstrate that fuel decomposition can promote forced ignition in fuel-lean  $C_{10}H_{22}$ /air mixtures while it has little effect on the stoichiometric case.

It is worth noting that for laser and spark ignition experiments, the decrease in MIE is less than that for simulations. That is because in simulations, a number of simplifications are involved in representing the localised ignition in numerical studies (e.g. neglecting the plasma formation, shock wave, heat loss to electrodes), which preclude a direct comparison of the minimum ignition energy obtained from experiments with computational results (the difference could be in one-order of magnitude according to previous studies, e.g. [42]). However, in spite of the above limitations, the experimental results qualitatively demonstrate the validity of some important conclusions drawn from numerical results. Furthermore, since the Markstein length and Lewis number of the mixture is reduced by fuel decomposition, the thermal-diffusion instability becomes stronger. The cellular structure may appear earlier in practical combustion engines.

## 5. Conclusions

One-dimensional transient simulations with detailed chemistry and transport are conducted to assess the effects of fuel decomposition on forced ignition in both homogenous and fuel-stratified mixtures. For homogeneous n-decane/air mixtures, fuel decomposition can greatly promote ignition for fuel-lean case while it has little effect for stoichiometric case. There exists a lower limit for the MIE, around which further increase in fuel decomposition does not further reduce the MIE. Four distinct flame regimes are identified and it is found that the duration of the unsteady flame transition regime is shortened by fuel decomposition. The combination of fuel decomposition and fuel stratification can further promote forced ignition. A fuel-stratification-induced ignition kernel propagation regime is observed. There exists an optimum stratification radius, and to promote the forced ignition only the fuel within the optimum stratification radius needs to be decomposed. The optimum stratification radius is found to increase as the fuel decomposition fraction decreases. Furthermore, laser and spark ignition experiments are conducted for  $C_{10}H_{22}/C_2H_4$ /air mixtures. The experimental results demonstrate the validity of some conclusions drawn from simulation results.

The forced ignition process in practical combustion engines is much more complicated than the present model. Here, as a first step, the simplified forced ignition process in a quiescent mixture is considered. Nevertheless, the present results provide useful guidance to the understanding how fuel decomposition affects the forced ignition. As an extension of the present work, future study needs include steady incoming flow and its effects on forced ignition.

## Acknowledgements

This work was supported by National Natural Science Foundation of China (Nos. 51861135309 and 91841302).



## Disclosure statement

No potential conflict of interest was reported by the author(s).

## Funding

This work was supported by National Natural Science Foundation of China [grant number 51861135309, 91841302].

## ORCID

Zheng Chen  <http://orcid.org/0000-0001-7341-6099>

## References

- [1] E. Daniau, M. Bouchez, R. Bounaceur, B.F. Leclerc, M.P. Marquaire, and R. Fournet, *Contribution to Scramjet active cooling analysis using N-dodecane decomposition model*, 12th AIAA International Space Planes and Hypersonic Systems and Technologies, 2003.
- [2] D. Zhang, L. Hou, J. Huo, J. Liu, and Z. Ren, *Investigation of the composition and laminar flame speed of pyrolysis gases*. J. Propul. Power 35 (2019), pp. 1065–1072.
- [3] Y. Yuan, T. Zhang, Y. Wei, and X. Fan, *Study on flame stabilization in a dual-mode combustor using optical measurements*. J. Propul. Power 31 (2015), pp. 1524–1531.
- [4] H. Wang, R. Xu, K. Wang, C.T. Bowman, R.K. Hanson, D.F. Davidson, K. Brezinsky, and F.N. Egolfopoulos, *A physics-based approach to modeling real-fuel combustion chemistry – I. Evidence from experiments, and thermodynamic, chemical kinetic and statistical considerations*. Combust. Flame 193 (2018), pp. 502–519.
- [5] J. Smolke, F. Carbone, F.N. Egolfopoulos, and H. Wang, *Effect of n-dodecane decomposition on its fundamental flame properties*. Combust. Flame 190 (2018), pp. 65–73.
- [6] X. You, H. Wang, and F.N. Egolfopoulos, *Detailed and simplified kinetic models of n-dodecane oxidation: the role of fuel cracking in aliphatic hydrocarbon combustion*. Proc. Combust. Inst. 32 (2009), pp. 403–410.
- [7] S.G. Davis and C.K. Law, *Determination of and fuel structure effects on laminar flame speeds of C1 to C8 hydrocarbons*. Combust. Sci. Technol. 140 (1998), pp. 427–449.
- [8] Z. Zhao, J. Li, A.F. Kazakov, F.L. Dryer, and S. Zeppieri, *Burning velocities and a high-temperature skeletal kinetic model for n-decane*. Combust. Sci. Technol. 177 (2004), pp. 89–106.
- [9] B. Zhong and H. Peng, *Experimental study on the combustion of thermally cracked endothermic hydrocarbon fuel*. Combust. Sci. Technol. 192 (2008), pp. 213–228.
- [10] B. Lewis and G.V. Elbe, *Combustion, flames and explosions of gases*, 3rd ed., Academic Press, New York, 1987.
- [11] Z. Chen and Y. Ju, *Theoretical analysis of the evolution from ignition kernel to flame ball and planar flame*. Combust. Theor. Model 11 (2007), pp. 427–453.
- [12] Z. Chen, M.P. Burke, and Y. Ju, *On the critical flame radius and minimum ignition energy for spherical flame initiation*. Proc. Combust. Inst. 33 (2011), pp. 1219–1226.
- [13] H. Zhang, P. Guo, and Z. Chen, *Critical condition for the ignition of reactant mixture by radical deposition*. Proc. Combust. Inst. 34 (2013), pp. 3267–3275.
- [14] A.C. Alkidas, *Combustion advancements in gasoline engines*. Energy Convers. Manage. 48 (2007), pp. 2751–2761.
- [15] M. Aliramezani, I. Chitsaz, and A.A. Mozafari, *Thermodynamic modeling of partially stratified charge engine characteristics for hydrogen-methane blends at ultra-lean conditions*. Int. J. Hydrogen Energy 38 (2013), pp. 10640–10647.
- [16] Y. Wang, W. Han, and Z. Chen, *Effects of fuel stratification on ignition kernel development and minimum ignition energy of n-decane/air mixtures*. Proc. Combust. Inst. 37 (2019), pp. 1623–1630.
- [17] Z. Chen, M.P. Burke, and Y. Ju, *Effects of Lewis number and ignition energy on the determination of laminar flame speed using propagating spherical flames*. Proc. Combust. Inst. 32 (2009), pp. 1253–1260.

- [18] Z. Chen, *Effects of radiation and compression on propagating spherical flames of methane/air mixtures near the lean flammability limit*. Combust. Flame 157 (2010), pp. 2267–2276.
- [19] R.J. Kee, F.M. Rupley, and J.A. Miller, *CHEMKIN-II: a Fortran package for the analysis of gas-phase chemical kinetics*, Sandia National Laboratory Rep. SAND89-8009B, 1989.
- [20] R.J. Kee, J.F. Grcar, M.D. Smooke, and J.A. Miller, *A Fortran program for modeling steady laminar one-dimensional premixed flames*, Sandia National Laboratory Rep. SAND85-8240, 1985.
- [21] M. Chaos, A.F. Kazakov, Z. Zhao, and F.L. Dryer, *A high-temperature chemical kinetic model for primary reference fuels*. Int. J. Chem. Kinet. 39 (2007), pp. 399–414.
- [22] P.N. Brown, G.D. Byrne, and A.C. Hindmarsh, *Vode: a variable-coefficient Ode solver*. SIAM J. Sci. Stat. Comput. 10 (1989), pp. 1038–1051.
- [23] W. Zhang, M. Faghih, X. Gou, and Z. Chen, *Numerical study on the transient evolution of a premixed cool flame*. Combust. Flame 187 (2018), pp. 129–136.
- [24] M. Faghih, W. Han, and Z. Chen, *Effects of soot diffusion on premixed flame propagation under engine-relevant conditions*. Combust. Flame 194 (2018), pp. 175–179.
- [25] Z. Chen, *Effects of radiation absorption on spherical flame propagation and radiation-induced uncertainty in laminar flame speed measurement*. Proc. Combust. Inst. 36 (2017), pp. 1129–1136.
- [26] W. Zhang, Z. Chen, and W. Kong, *Effects of diluents on the ignition of premixed H<sub>2</sub>/air mixtures*. Combust. Flame 159 (2012), pp. 151–160.
- [27] T.M. Sloane and P.D. Ronney, *A comparison of ignition phenomena modelled with detailed and simplified kinetics*. Combust. Sci. Technol. 88 (1993), pp. 1–13.
- [28] S.M. Sarathy, C.K. Westbrook, M. Mehl, W.J. Pitz, C. Togbe, P. Dagaut, H. Wang, M.A. Oehlschlaeger, U. Niemann, and K. Seshadri, *Comprehensive chemical kinetic modeling of the oxidation of 2-methylalkanes from C7 to C20*. Combust. Flame 158 (2011), pp. 2338–2357.
- [29] T. Malewicki and K. Brezinsky, *Experimental and modeling study on the pyrolysis and oxidation of n-decane and n-dodecane*. Proc. Combust. Inst. 34 (2013), pp. 361–368.
- [30] T. Malewicki, A. Comandini, and K. Brezinsky, *Experimental and modeling study on the pyrolysis and oxidation of iso-octane*. Proc. Combust. Inst. 34 (2013), pp. 353–360.
- [31] W. Shen, Y. Zhang, B. Zhao, D. Chang, J. Lyu, and H. Zhang, *Experimental and modelling studies on pyrolysis and its main light gas products for typical C8 hydrocarbons*. J. Anal. Appl. Pyrolysis 142 (2019), pp. 104622.
- [32] H.H. Kim, H.W. Sang, J. Santner, Z. Chen, and Y. Ju, *Measurements of the critical initiation radius and unsteady propagation of n-decane/air premixed flames*. Proc. Combust. Inst. 34 (2013), pp. 929–936.
- [33] J.S. Santner, H.W. Sang, and Y. Ju, *Chemistry and transport effects on critical flame initiation radius for alkanes and aromatic fuels*. Proc. Combust. Inst. 36 (2016), pp. 1457–1465.
- [34] Z. Chen, *On the extraction of laminar flame speed and Markstein length from outwardly propagating spherical flames*. Combust. Flame 158 (2011), pp. 291–300.
- [35] Z. Chen, *On the accuracy of laminar flame speeds measured from outwardly propagating spherical flames: methane/air at normal temperature and pressure*. Combust. Flame 162 (2015), pp. 2442–2453.
- [36] D. Patel and N. Chakraborty, *Localised forced ignition of globally stoichiometric stratified mixtures: A numerical investigation*. Combust. Theor. Model 18 (2014), pp. 627–651.
- [37] D. Patel and N. Chakraborty, *Effects of mixture distribution on localized forced ignition of stratified mixtures: a direct numerical simulation study*. Combust. Sci. Technol. 188 (2016), pp. 1904–1924.
- [38] N. Mokrani and P. Gillard, *Laser induced breakdown in gas mixtures. Experimental and statistical investigation on n-decane ignition: pressure, mixture composition and equivalence ratio effects*. J. Hazard. Mater. 388 (2020), pp. 119266.
- [39] S. Rudz and P. Gillard, *Effect of initial laser beam diameter on breakdown and ignition properties of n-decane/N<sub>2</sub>/O<sub>2</sub> mixtures*. Combust. Sci. Technol. 191 (2019), pp. 284–295.

- [40] S. Rudz, P. Tadini, F. Berthet, and P. Gillard, *Effect of low initial pressures on ignition properties of lean and rich n-decane/air mixtures for laser-induced breakdown*. Combust. Sci. Technol. 191 (2019), pp. 223–242.
- [41] B. Lin, Y. Wu, Z. Zhang, and Z. Chen, *Multi-channel nanosecond discharge plasma ignition of premixed propane/air under normal and sub-atmospheric pressures*. Combust. Flame 182 (2017), pp. 102–113.
- [42] P.D. Ronney, *Laser versus conventional ignition of flames*. Opt. Eng. 33 (1994), pp. 510–521.